Bruno Exposto, Rui Rodrigues, J. G. Pinto, Vítor Monteiro, João L. Afonso

**“Predictive Control of a Current-Source Inverter for Solar Photovoltaic Grid Interface”**

CPE International Conference on Compatibility and Power Electronics, Lisboa Portugal.

http://ieeexplore.ieee.org/stamp/stamp.jsp?tp=&arnumber=7231058

**ISBN**: 978-1-4799-6300-3

**DOI** 10.1109/CPE.2015.7231058

Bruno Exposto, Rui Rodrigues, J. G. Pinto, Vítor Monteiro, João L. Afonso, "Predictive Control of a Current-Source Inverter for Solar Photovoltaic Grid Interface," CPE International Conference on Compatibility and Power Electronics, Lisboa Portugal, pp.113-118, June 2015. ISBN: 978-1-4799-6300-3. DOI: 10.1109/CPE.2015.7231058

# Predictive Control of a Current-Source Inverter for Solar Photovoltaic Grid Interface

Bruno Exposto, Rui Rodrigues, J. G. Pinto, Vítor Monteiro, Delfim Pedrosa, João L. Afonso
ALGORITMI Research Centre – University of Minho, Guimarães – Portugal
{bruno.exposto | rui.rodrigues | gabriel.pinto | vitor.monteiro |delfim.pedrosa | joao.l.afonso}@algoritmi.uminho.pt

***Abstract*— Solar photovoltaic systems are an increasing option for electricity production, since they produce electrical energy from a clean renewable energy resource, and over the years, as a result of the research, their efficiency has been increasing. For the interface between the dc photovoltaic solar array and the ac electrical grid is necessary the use of an inverter (dc-ac converter), which should be optimized to extract the maximum power from the photovoltaic solar array. In this paper is presented a solution based on a current-source inverter (CSI) using continuous control set model predictive control (CCS-MPC). All the power circuits and respective control systems are described in detail along the paper and were tested and validated performing computer simulations. The paper shows the simulation results and are drawn several conclusions.**

***Keywords—Solar Photovoltaics; Current Source Inverter; Predictive Control; Maximum Power Point Tracker - MPPT.***

## I. INTRODUCTION

The problems associated with climate change and those associated with the massive use of fossil fuels are leading to the necessity of find new energy sources. Although that exist research in another areas with new energy sources, renewable energy sources are at the moment an excellent alternative to conventional energy sources. The main advantages of those energy sources are the lower environmental impact, and the fact that take advantage of natural resources. Today, it is possible to see several countries of the world establishing ambitious goals in terms of renewable energy share in a near future. The European Union [1], China [2] and even United States [3][4] are examples of what is happening is this field.

Until sometime ago, the main share in the area of renewable energy was hydroelectric energy, being therefore, wind and solar energy the two most promising renewable energy sources [5]. Alongside with large wind, solar photovoltaic renewable energy sources has been increasingly explored in recent years. The prices either of the solar photovoltaic panels, as well as the price of the power converters, have been consistently lowering [2][6], enabling its expansion and opening new possibilities in terms of the energetic paradigm such as the prosumer [7]. Today's solar photovoltaic systems integrate a solar array and power electronics systems that allow perform the power conversion from the solar photovoltaic arrays to the electrical grid. Solar photovoltaic systems can be classified in terms of power and in terms of the type of power converters that constitute it [3]. Although the main adopted inverter topology for solar photovoltaic systems is the voltage-source inverter (VSI), current-source inverters (CSI) applied to solar photovoltaic systems were also studied [8][9]. Current-source inverters have been used in other power electronics applications such as active filters, motor drives and renewable energy applications [10][11]. The advantages of this type of inverter are the good quality output currents and the fact of being robust [12]. The disadvantages are the bulky dc-link inductance, and the increased dc-link energy losses.

In this paper is proposed the use of a current source inverter with the dc link inductance connected directly to the solar photovoltaic to perform the interface between the electrical grid and a solar photovoltaic array. The control of the solar photovoltaic CSI, integrates a maximum power point tracker (MPPT) and a continuous control set model predictive control (CCS-MPC) to control the inverter output currents. Although that MPC has been extensively researched over the years, the application of this type of control to solar photovoltaic systems with current-source inverters can be further studied and developed. The use of CCS-MPC can bring several advantages to the operation of the solar photovoltaic CSI, because has good dynamics and ensures a fixed switching frequency [13].

## II. CURRENT-SOURCE INVERTER TOPOLOGY

The topology of the proposed inverter is a three-phase current-source inverter (Fig. 1). The power switches in the inverter are IGBTs with power diodes placed in series. This is necessary because in a current-source inverter, the power switches must withstand direct and reverse voltages. The passive

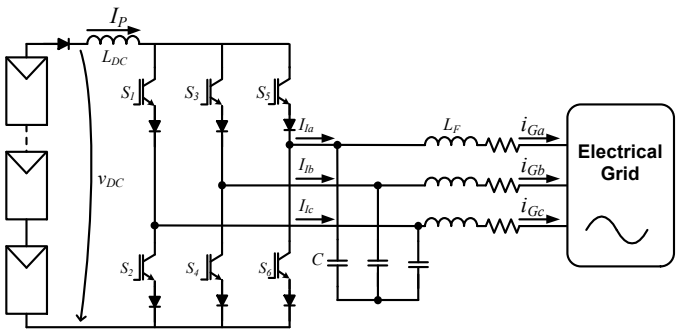


Fig. 1. Topology of the three-phase current source inverter for solar photovoltaic applications.

filters are LC filters. The three-phase current-source inverter is responsible by inject the energy drawn from the solar photovoltaic panels into the electrical grid. The current control is performed measuring the currents $i_{G\{a,b,c\}}$ and the grid voltages $v_{G\{a,b,c\}}$.

### A. Dc-link Inductance

The solar photovoltaic array is constituted by a series of BP Solar BP2150S. Each one of this panels has 72 monocrystalline silicon solar cells placed in series. The characteristics of this panel can be seen in Table 1.

Considering that the solar photovoltaic panels have a behavior similar to a current source, in this application was used a three-phase current-source inverter. With this converter is possible apply directly the photovoltaic array in the dc-link, excluding the use of another converter, even with the variation of the voltage of the photovoltaic array. While a three-phase voltage-source inverter needs, to guarantee a proper operation, a dc-link voltage of $\sqrt{2}\,V_{L-L}$, greater than the peak value of the power grid line to line voltage i.e. about 565 V for a 400 V power grid i.e., about 565 V, the current-source inverter only needs 66% of that voltage [14]. To ensure this voltage, was considered a solar array constituted by two parallel arrays with a total of 22 panels, each one with 34 V, making a total voltage of 374 V, and a total power of 3300 W.

Considering that the dc-link current ripple must be the lowest possible, ensuring that the maximum power is extracted from the solar photovoltaic array, was calculated the minimum dc-link inductance value necessary to ensure a defined current ripple using [15]:

$$L_{DC,\min.} = \frac{\sqrt{6}}{2}\frac{V_{DC}}{f_S \Delta i_{d,\max.}}, \tag{1}$$

where $v_{DC}$ is the inverter input voltage, $f_s$ is the switching frequency of the converter, and $\Delta i_{d,\max.}$ is the maximum admissible current ripple. In Fig. 2 it is possible to see a graph that shows the relation between the aforementioned variables. In this case was considered as voltage value, the total voltage of the solar array and a switching frequency is 32 kHz. Finally, the maximum admitted ripple is 0.3 A.

## III. Inverter Control

The most common current control schemes are based in linear controllers such as: linear controller in a-b-c reference frame [16] and linear controller in $\alpha$-$\beta$ reference frame [17][18].

TABLE I.
BP Solar Panel BP2150S Characteristics

| Parameter | Symbol | Value |
|---|---|---|
| Maximum Power | $P_m$ | 150 W |
| Voltage at $P_m$ | $V_{mpp}$ | 34.0 V |
| Current at $P_m$ | $I_{mpp}$ | 4.45 A |
| Short Circuit Current | $I_{sc}$ | 4.75 A |
| Open Circuit Voltage | $V_{oc}$ | 42.8 V |
| $I_{sc}$ Temperature Coeficient | $\alpha$ | (0.065±0.015) %/°C |
| $V_{oc}$ Temperature Coeficient | $\beta$ | -(160±20) mV/°C |

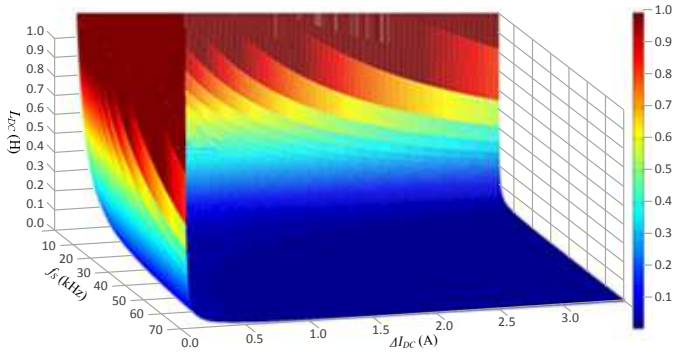


Fig. 2. Dc-link inductance ($L_{DC}$) value *vs* current ripple ($\Delta i_{DC}$) and switching frequency ($F_S$).

In these control schemes is assumed that the model of the system is linear and invariant in time (LIT) and is also that is known with some degree of confidence. In this case, the inverter current control is performed using CCS-MPC with a fixed frequency modulation technique. Although that, most of the MPC is implemented imposing a variable switching frequency by minimizing the error between the reference current and the inverter current [19], is possible implement this type of current control using a fixed frequency. This presents some advantages such as a simple passive filter design and a simple protection mechanism of the power semiconductors [20].

### A. Current Control and Modulation Technique

The inverter reference currents, are generated multiplying the signals obtained with a phase-locked loop (PLL) with the MPPT algorithm output signals (2)(3). The PLL is necessary to synchronize the output currents of the inverter ($i_{G\{a,b,c\}}$) with the positive sequence of the fundamental components of the grid voltages.

$$i^*_{G\alpha} = v^+_{\alpha 1}\, k_{MPPT} \tag{2}$$

$$i^*_{G\beta} = v^+_{\beta 1}\, k_{MPPT} \tag{3}$$

After this is necessary calculate the predicted inverter output currents. To do this, is necessary develop on the dynamics of the system considering Fig. 3, which can be expressed as:

$$\begin{aligned} i_{I\{\alpha,\beta\}} &= i_{C\{\alpha,\beta\}} + i_{G\{\alpha,\beta\}}, \\ v_{C\{\alpha,\beta\}} &= v_{G\{\alpha,\beta\}} + v_{LF\{\alpha,\beta\}} + v_{RF\{\alpha,\beta\}}. \end{aligned} \tag{4}$$

If we combine the two aforementioned equations it yields (5).

$$L_F C \frac{d^2 i_{G\{\alpha,\beta\}}}{dt^2} + R_F C \frac{d i_{G\{\alpha,\beta\}}}{dt} + i_{G\{\alpha,\beta\}} + \tag{5}$$

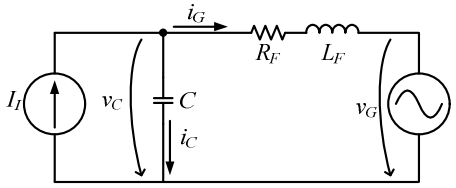


Fig. 3. Current-source inverter and passive filter model.

$$+C\frac{dv_{G\{\alpha,\beta\}}}{dt}-I_I=0\,.$$

Using the backward Euler method, and considering a sampling frequency $T_S$, is possible discretize the system as:

$$\begin{aligned}&\frac{CL_F}{T_S^2}\left(i_{G\{\alpha,\beta\}}[n-2]-2i_{G\{\alpha,\beta\}}[n-1]+i_{G\{\alpha,\beta\}}[n]\right)+\\&\frac{CR_F}{T_S}\left(i_{G\{\alpha,\beta\}}[n]-i_{G\{\alpha,\beta\}}[n-1]\right)+i_{G\{\alpha,\beta\}}[n]+\\&+\frac{C}{T_S}\left(v_{G\{\alpha,\beta\}}[n]-v_{G\{\alpha,\beta\}}[n-1]\right)-I_I[n]=0\,.\end{aligned}\tag{6}$$

Rearranging the terms is possible obtain:

$$\begin{aligned}&k_1 i_{G\{\alpha,\beta\}}[n-2]+k_2 i_{G\{\alpha,\beta\}}[n-1]+k_3 i_{G\{\alpha,\beta\}}[n]+\\&k_4\left(v_{G\{\alpha,\beta\}}[n]-v_{G\{\alpha,\beta\}}[n-1]\right)-I_I[n]=0\,,\end{aligned}\tag{7}$$

where,

$$\begin{aligned}&k_1=\frac{CL_F}{T_S^2}\,,\ k_2=-\frac{(R_F T_S+2L_F)C}{T_S^2}\,,\\&k_3=\frac{(R_F T_S+L_F)C+T_S^2}{T_S^2}\,,\ k_4=\frac{C}{T_S}\,.\end{aligned}\tag{8}$$

Considering that the objective is that the error in sample *n+1* between the reference current and the injected current is to be zero, the problem can be stated as:

$$\begin{aligned}&k_1 i_{G\{\alpha,\beta\}}[n-1]+k_2 i_{G\{\alpha,\beta\}}[n]+k_3 i_{G\{\alpha,\beta\}}[n+1]+\\&k_4\left(v_{G\{\alpha,\beta\}}[n+1]-v_{G\{\alpha,\beta\}}[n]\right)-I_I[n+1]=0\,.\end{aligned}\tag{9}$$

Making $i_{G\{\alpha,\beta\}}[n+1]=i^*_{G\{\alpha,\beta\}}[n]$ and considering the present and past values of the system, the current that must be injected by the inverter can be calculated as:

$$\begin{aligned}I_I[n+1]=&\,k_1 i_{G\{\alpha,\beta\}}[n-1]+k_2 i_{G\{\alpha,\beta\}}[n]+k_3 i^*_{G\{\alpha,\beta\}}[n]+\\&+k_4\left(v_{G\{\alpha,\beta\}}[n+1]-v_{G\{\alpha,\beta\}}[n]\right)\,.\end{aligned}\tag{10}$$

The voltage $v_{G\{\alpha,\beta\}}[n+1]$ can be estimated as:

$$v_{G\{\alpha,\beta\}}[n+1]=2v_{G\{\alpha,\beta\}}[n]-v_{G\{\alpha,\beta\}}[n-1]\,.\tag{11}$$

To insure that the current-source inverter is always stable, was implemented a damping algorithm based in the virtual capacitor voltage ($v_C$) divided by a virtual resistance ($R_h$) as:

$$i_D=\frac{1}{R_h}\left(v_{G\{\alpha,\beta\}}[n]+\frac{L_F}{T_S}\left(i_{G\{\alpha,\beta\}}[n]-i_{G\{\alpha,\beta\}}[n-1]\right)\right).\tag{12}$$

The damping current is introduced in a high-pass digital filter, and then is added to the reference current of the modulation block. In this way is only measured the grid voltages, requiring only three voltage sensors and the output currents. It must be referred that this damping strategy

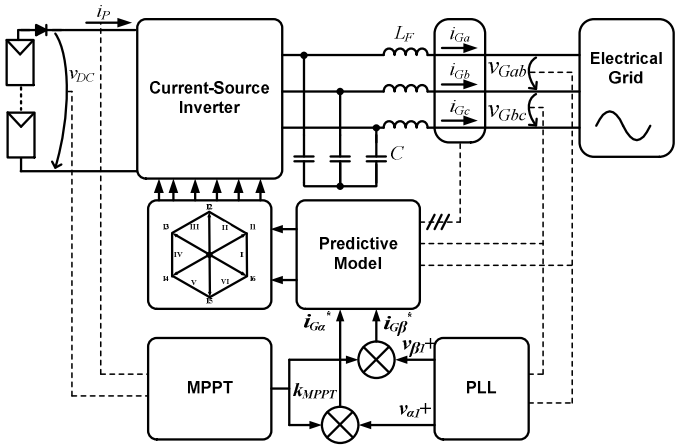


Fig. 4. Block diagram of the Photovoltaic CSI controller.

effectiveness is dependent of the sampling frequency of the analogue-to-digital converters (ADC). In Fig. 5 is shown a control diagram resuming the control strategies that were presented in this section.

Finally, considering that the passive filter introduces reactive power in the power grid, it was implemented a loop in the control that eliminates this. To perform this task is calculated the average value of the reactive power ($\bar{q}$) in the output of the inverter as:

$$\bar{q}[n]=\frac{1}{N}\sum_{n=0}^{n=N} v_{G\beta}[n]\,i_{G\alpha}[n]+v_{G\alpha}[n]\,i_{G\beta}[n]\,,\tag{13}$$

where *N* is the number of samples of one grid cycle. The predictive control reference current will be then:

$$\begin{aligned}i_\alpha[n]&=i^*_{G\alpha}[n]-\frac{v_{G\beta}[n]\,\bar{q}[n]}{v^2_{G\alpha}[n]+v^2_{G\beta}[n]}\,,\\i_\beta[n]&=i^*_{G\beta}[n]+\frac{v_{G\alpha}[n]\,\bar{q}[n]}{v^2_{G\alpha}[n]+v^2_{G\beta}[n]}\,.\end{aligned}\tag{14}$$

Having calculated the predicted reference current, the next step will be modulate the output currents. To do this was implemented a space-vector modulator, with a fixed switching frequency of 32 kHz. Having the reference currents in the *α-β* reference frame, the next step will be to find the sector in which is the current reference vector (Fig. 6). After this will be calculated the times ($t_0$, $t_1$ and $t_2$) during what will be applied the

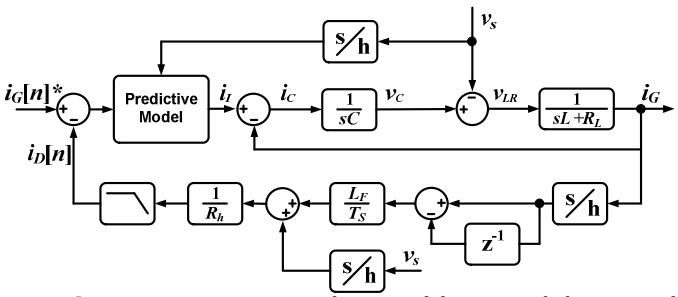


Fig. 5. Current-source inverter equivalent control diagram, with the integrated damping mechanism.

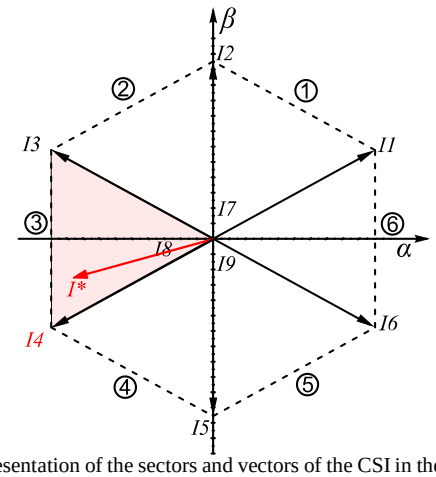


Fig. 6. Representation of the sectors and vectors of the CSI in the $\alpha$-$\beta$ reference frame.

vectors, that constitute the boundaries of the sector. In table 3 it is possible to see all the valid states of the current-source inverter. It must be referred that vectors *I7*, *I8*, *I9* are null vectors and are placed in the center of the $\alpha$-$\beta$ reference frame.

### *B. Maximum Power Point Tracker*

To ensure that the maximum available power of the panels is injected into the electrical grid in every moment, is necessary implement a maximum power point tracker (MPPT). In the literature are described several MPPTs, each one with advantages and disadvantages. Also exist several methods to implement the MPPT, depending on the type of the adopted power converter or power converters. In some works the MPPT is associated with a proportional-integral (PI) controller [21]. In this case is proposed the direct connection between the MPPT algorithm and the reference output currents, as is presented in Fig. 4. Considering that the inverter is a current-source inverter the reference currents are more easily followed ensuring that the MPPT operates correctly. Also because was implemented a predictive current control, is expected that the inverter control reacts faster to the changing of the reference currents.

The adopted algorithm was the Incremental Conductance. This method is more complex than other methods, but it has a good performance [22]. Furthermore, this is a true MPPT and

TABLE II.
CSI VALID STATES AND VECTORS

| Vector | $i_{INVa}$ | $i_{INVb}$ | $i_{INVc}$ | $i_{INVn}$ | $i_\alpha$ | $i_\beta$ | Active Switches |
|---|---|---|---|---|---|---|---|
| 1 | $+I_P$ | 0 | $-I_P$ | 0 | 1 | $1/\sqrt{3}$ | S1, S2 |
| 2 | 0 | $+I_P$ | $-I_P$ | 0 | 0 | $2/\sqrt{3}$ | S2, S3 |
| 3 | $-I_P$ | $+I_P$ | 0 | 0 | -1 | $1/\sqrt{3}$ | S3, S4 |
| 4 | $-I_P$ | 0 | $+I_P$ | 0 | -1 | $-1/\sqrt{3}$ | S4, S5 |
| 5 | 0 | $-I_P$ | $+I_P$ | 0 | 0 | $-2/\sqrt{3}$ | S5, S6 |
| 6 | $+I_P$ | $-I_P$ | 0 | 0 | 1 | $-1/\sqrt{3}$ | S6, S1 |
| 7 | 0 | 0 | 0 | 0 | 0 | 0 | S1, S4 |
| 8 | 0 | 0 | 0 | 0 | 0 | 0 | S3, S6 |
| 9 | 0 | 0 | 0 | 0 | 0 | 0 | S5, S2 |

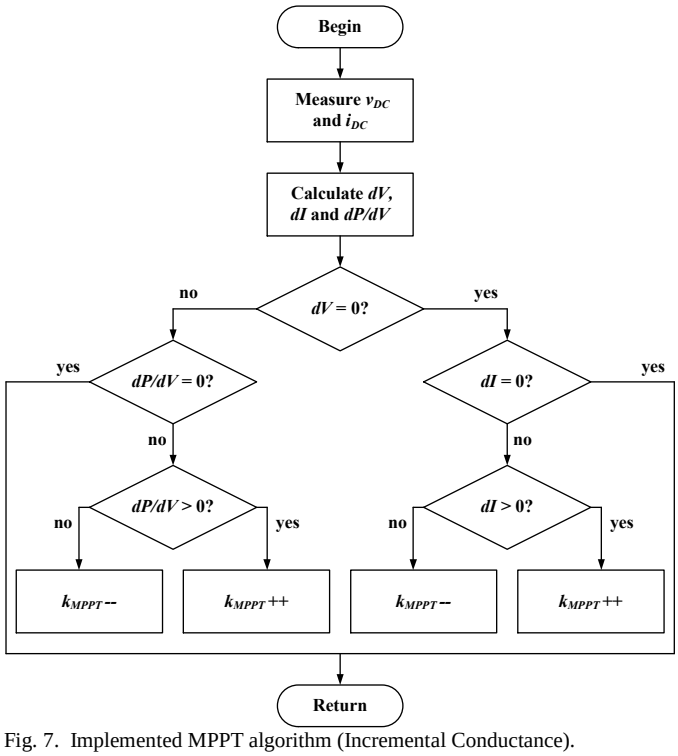


Fig. 7. Implemented MPPT algorithm (Incremental Conductance).

when the maximum power point (MPP) is reached, the algorithm stays in that operating point, until some change is detected [23]. To implement this algorithm is necessary to measure the voltage in the input of the inverter ($v_{DC}$) and output current ($i_P$). In Fig. 7 it is possible to see the flowchart of the implemented MPPT algorithm.

## IV. Simulation Results

In order to determine the performance of the solar photovoltaic current-source inverter with the proposed control was developed a simulation model similar to what is depicted in Fig. 1. The model parameter values are shown in Table III. It must be referred that the simulation results were obtained using the software PSIM from POWERSIM.

In Fig. 8 can be seen the simulation results, more specifically the output currents of the inverter, when operates at the solar photovoltaic panels maximum power, the dc-link inductance current, and the photovoltaic array voltage. As can be seen, in Fig. 8 (b), the grid currents ($i_G$) are sinusoidal and in opposite phase with the grid voltages ($v_G$) (Fig. 8 (a)). This shows that the

TABLE III
PHOTOVOLTAIC CSI SIMULATION MODEL PARAMETERS

| Parameter | Symbol | Value |
|---|---|---|
| CSI dc-link inductor | $L_{DC}$ | 70 mH |
| Passive filter inductor | $L_F$ | 6 mH |
| Passive filter capacitor | $C_F$ | 60 µF |
| Passive filter resistance | $R_F$ | 0.3 Ω |
| Inverter switching frequency | $F_S$ | 32 kHz |
| Grid voltage (rms) | $V_G$ | 230 V |
| Grid frequency | $F$ | 50 Hz |

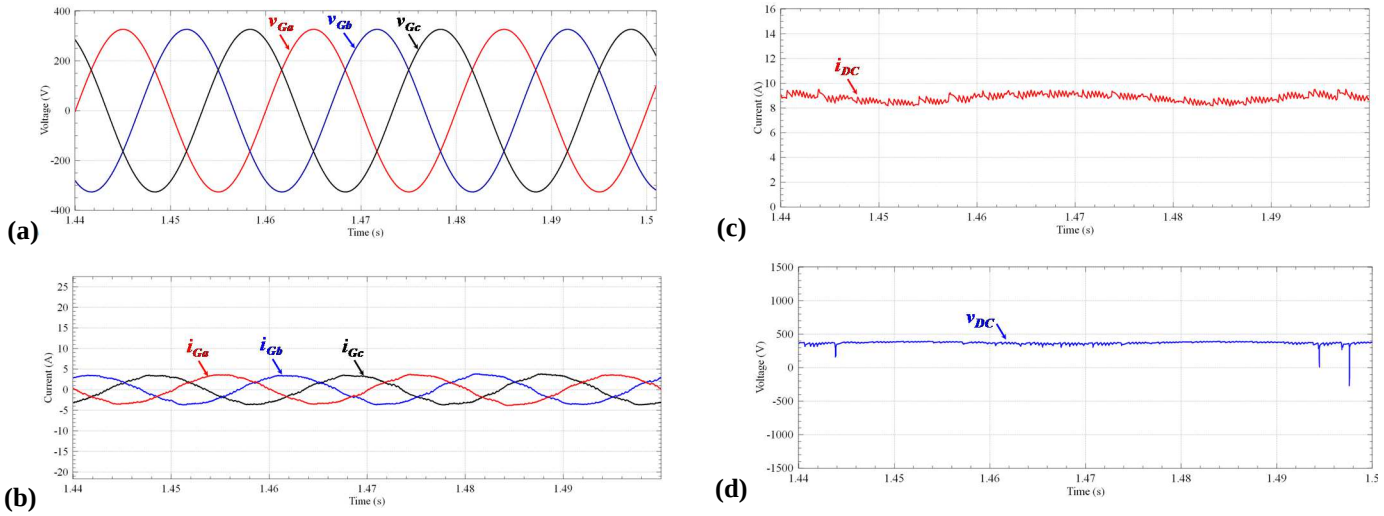


Fig. 8. Simulation results of the solar photovoltaic CSI injecting energy from the solar photovoltaic arrays: (a) Grid voltages ($v_G$); (b) Grid currents ($i_G$); (c) dc-link inductance current; (d) dc-link voltage.

CCS-MPC is operating correctly and that the grid is absorbing the power generated by the photovoltaic array. In this figure is also possible to see the dc-link current ($i_{DC}$) and the voltage in the input of the inverter ($v_{DC}$). The ripple of the dc-link current is low, as expected.

Fig. 10 shows the phase A reference current ($i_{Ga}$*) and the injected current ($i_{Ga}$*). The reference current is followed correctly by the inverter. It must be referred that, because the MPPT is controlling directly the amplitude of the output currents, the response to the variation of $k_{MPPT}$ is fast. Nevertheless the choice of the incrementing step of the MPPT can affect the distortion of the output currents.

The simulation results of the MPPT algorithm operation are shown in Fig. 9. The figure shows that the MPPT algorithm tracks effectively the operation power of the solar photovoltaic array. In Fig. 9 (a) it is possible to see the converter input power ($P_C$) and the photovoltaic array available power ($P_P$). The figure shows the increments of the MPPT variable, $k_{MPPT}$ over the time, and its stabilization around the maximum power point. In the beginning of the simulation, the input power is oscillating, but this is related with the stabilization of the model.

## V. Conclusions

In this paper was presented a current-source inverter (CSI) for the interface between the photovoltaic solar array and the electrical grid with an integrated maximum power point tracker (MPPT). The control of the inverter is performed using continuous control set model predictive control to control the output inverter currents. The control algorithms of the inverter are described and are analyzed. Also, are presented the simulation results obtained with a developed model, which show that the current-source inverter operates correctly when injecting energy into the electrical power grid.

It is also shown that the MPPT is capable of tracking the solar photovoltaic array available power.

In the future will be implemented a prototype of the proposed CSI for solar photovoltaic grid interface in order to obtain experimental results. This will allow to confirm the simulation results and better assess the behavior of the proposed equipment and control algorithms. Also, it will allow determine the

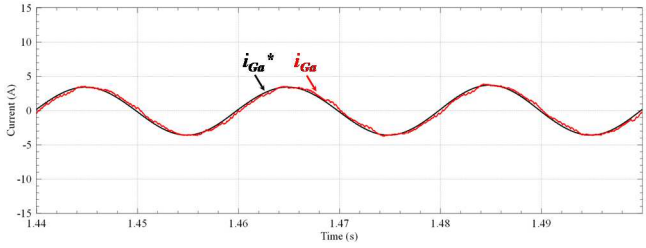


Fig. 10. Simulation results of the CSI inverter reference current ($i_{Ga}^*$) and inverter current ($i_{Ga}$).

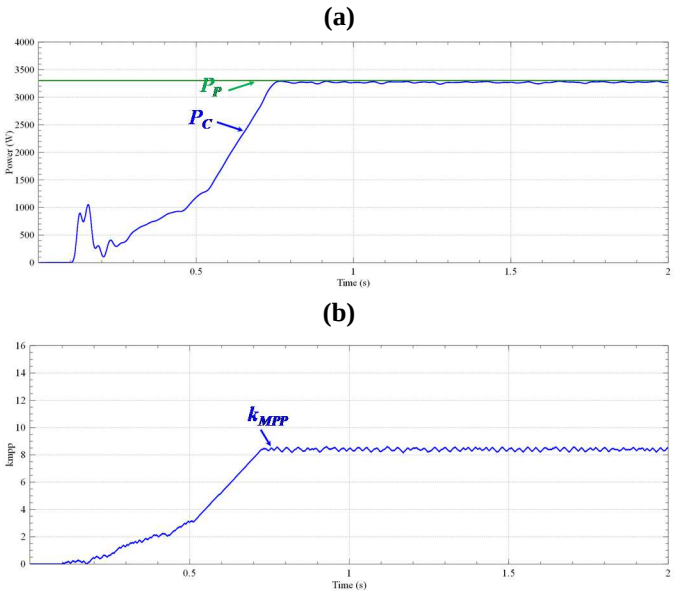


Fig. 9. Simulation results of the MPPT algorithm: (a) Inverter input power ($P_i$) and optimum power $P_P$; (b) MPPT control variable ($k_{MPPT}$).

efficiency of the inverter operating with the CCS-MPC current control.

## ACKNOWLEDGMENT

This work has been supported by FCT - Fundação para a Ciência e Tecnologia within scope of the project: PEst-UID/CEC/00319/2013. Bruno Exposto was supported by the doctoral scholarship SFRH/BD/87999/2012 granted by FCT.

## REFERENCES

[1] J. Holmes, "A More Perfect Union: Energy Systems Integration Studies from Europe," *Power and Energy Magazine, IEEE*, vol. 11, no. 5, pp. 36–45, 2013.

[2] X. Yang, Y. Song, G. Wang, and W. Wang, "A Comprehensive Review on the Development of Sustainable Energy Strategy and Implementation in China," *Sustainable Energy, IEEE Transactions on*, vol. 1, no. 2, pp. 57–65, 2010.

[3] F. Blaabjerg, F. Iov, T. Terekes, R. Teodorescu, and K. Ma, "Power Electronics – Key Technology for Renewable Energy Systems – Status and Future," in *Power Electronics, Drive Systems and Technologies Conference (PEDSTC), 2011 2nd*, 2011, pp. 445–466.

[4] A. E. Jones, M. Irwin, and A. Izadian, "Incentives for microgeneration development in the U.S. and Europe," in *IECON 2010 - 36th Annual Conference on IEEE Industrial Electronics Society*, 2010, pp. 3018–3021.

[5] M. Liserre, T. Sauter, and J. Y. Hung, "Future Energy Systems: Integrating Renewable Energy Sources into the Smart Power Grid Through Industrial Electronics," *Industrial Electronics Magazine, IEEE*, vol. 4, no. 1, pp. 18–37, 2010.

[6] S. B. Kjaer, J. K. Pedersen, and F. Blaabjerg, "A review of single-phase grid-connected inverters for photovoltaic modules," *Industry Applications, IEEE Transactions on*, vol. 41, no. 5, pp. 1292–1306, 2005.

[7] P. G. D. Silva, S. Karnouskos, and D. Ilic, "A Survey Towards Understanding Residential Prosumers in Smart Grid Neighbourhoods," in *Innovative Smart Grid Technologies (ISGT Europe), 2012 3rd IEEE PES International Conference and Exhibition on*, 2012, pp. 1–8.

[8] G. Ertasgin, D. M. Whaley, N. Ertugrul, and W. L. Soong, "A current-source grid-connected converter topology for Photovoltaic systems," in *Australasian Universities Power Engineering Conference. AUPEC'06.(2006: Melbourne, Australia)*, 2006.

[9] B. Sahan, A. Notholt-Vergara, A. Engler, and P. Zacharias, "Development of a single-stage three-phase PV module integrated converter," in *Proc. 12th European Conference on Power Electronics and Applications EPE, Aalborg, Denmark*, 2007.

[10] B. Exposto, J. Pinto, D. Pedrosa, V. Monteiro, H. Goncalves, and J. L. Afonso, "Current-Source Shunt Active Power Filter with Periodic-Sampling Modulation Technique," in *IECON 2012-38th Annual Conference on IEEE Industrial Electronics Society*, 2012, pp. 1274–1279.

[11] Y. Zhang and Y. W. Li, "Investigation and Suppression of Harmonics Interaction in High-Power PWM Current-Source Motor Drives," *Power Electronics, IEEE Transactions on*, vol. 30, no. 2, pp. 668–679, 2015.

[12] G. Ertasgin, "Low-Cost Current-Source 1-ph Photovoltaic Grid-Connected Inverter," 2010.

[13] M. Preindl and S. Bolognani, "Comparison of direct and PWM model predictive control for power electronic and drive systems," in *Applied Power Electronics Conference and Exposition (APEC), 2013 Twenty-Eighth Annual IEEE*, 2013, pp. 2526–2533.

[14] S. B. Kjaer, J. K. Pedersen, and F. Blaabjerg, "Evaluation of Single-Stage Power Converter Topologies for Grid-Connected Photovoltaics," *Industry Applications, IEEE Transactions on*, vol. 41, no. 5, pp. 1292–1306, 2005.

[15] F. W. Fuchs and A. Kloenne, "DC link and dynamic performance features of PWM IGBT current source converter induction machine drives with respect to industrial requirements," in *Power Electronics and Motion Control Conference, 2004. IPEMC 2004. The 4th International*, 2004, vol. 3, pp. 1393–1398 Vol.3.

[16] Z. Bai, H. Ma, D. Xu, B. Wu, Y. Fang, and Y. Yao, "Resonance Damping and Harmonic Suppression for Grid-Connected Current-Source Converter," *Industrial Electronics, IEEE Transactions on*, vol. 61, no. 7, pp. 3146–3154, 2014.

[17] J. W. G. Hwang, M. Winkelnkemper, and P. W. Lehn, "Design of an Optimal Stationary Frame Controller for Grid Connected AC-DC Converters," in *IEEE Industrial Electronics, IECON 2006 - 32nd Annual Conference on*, 2006, pp. 167–172.

[18] X. Yuan, W. Merk, H. Stemmler, and J. Allmeling, "Stationary-frame generalized integrators for current control of active power filters with zero steady-state error for current harmonics of concern under unbalanced and distorted operating conditions," *Industry Applications, IEEE Transactions on*, vol. 38, no. 2, pp. 523–532, 2002.

[19] I. Lizama, J. Rodriguez, B. Wu, P. Correa, M. Rivera, and M. Perez, "Predictive control for current source rectifiers operating at low switching frequency," in *Power Electronics and Motion Control Conference, 2009. IPEMC '09. IEEE 6th International*, 2009, pp. 1630–1633.

[20] P. Cortes, M. P. Kazmierkowski, R. M. Kennel, D. E. Quevedo, and J. Rodriguez, "Predictive Control in Power Electronics and Drives," *Industrial Electronics, IEEE Transactions on*, vol. 55, no. 12, pp. 4312–4324, 2008.

[21] A. K. Abdelsalam, A. M. Massoud, S. Ahmed, and P. Enjeti, "High-Performance Adaptive Perturb and Observe MPPT Technique for Photovoltaic-Based Microgrids," *Power Electronics, IEEE Transactions on*, vol. 26, no. 4, pp. 1010–1021, 2011.

[22] T. Esram and P. L. Chapman, "Comparison of photovoltaic array maximum power point tracking techniques," *IEEE TRANSACTIONS ON ENERGY CONVERSION EC*, vol. 22, no. 2, p. 439, 2007.

[23] K. S. Tey and S. Mekhilef, "Modified incremental conductance MPPT algorithm to mitigate inaccurate responses under fast-changing solar irradiation level," *Solar Energy*, vol. 101, pp. 333–342, 2014.